

# Evidence of Vortex Jamming in Abrikosov Vortex Flux Flow Regime

G. Karapetrov,<sup>1,\*</sup> V. Yefremenko,<sup>2</sup> G. Mihajlović,<sup>2,†</sup> J. E. Pearson,<sup>2</sup> M. Iavarone,<sup>3</sup> V. Novosad,<sup>2</sup> and S. D. Bader<sup>2</sup>

<sup>1</sup>*Department of Physics, Drexel University, 3141 Chestnut Street, Philadelphia, PA 19104, USA*

<sup>2</sup>*Materials Science Division, Argonne National Laboratory, Argonne, Illinois 60439, USA*

<sup>3</sup>*Department of Physics, Temple University, Philadelphia, PA 19122, USA*

(Dated: June 24, 2018)

We report on dynamics of non-local Abrikosov vortex flow in mesoscopic superconducting Nb channels. Magnetic field dependence of the non-local voltage induced by the flux flow shows that vortices form ordered vortex chains. Voltage asymmetry (rectification) with respect to the direction of vortex flow is evidence that vortex jamming strongly moderates vortex dynamics in mesoscopic geometries. The findings can be applied to superconducting devices exploiting vortex dynamics and vortex manipulation, including superconducting wires with engineered pinning centers.

PACS numbers: 74.25.Op, 74.25.Uv, 73.23.-b, 74.78.Na

The dynamic behavior of vortices in type-II superconductors is important in applications [1] and provides an exemplary model system. Abrikosov vortices in type-II superconductors are set in motion when the Lorentz force due to local supercurrents exceeds the strength of vortex pinning forces, resulting in energy dissipation. Therefore, control of the dynamic behavior of vortices has a broad relevance for reducing losses in superconducting wires and microwave devices. Also, the ability to control and manipulate single magnetic flux quanta could lead to novel superconducting devices, such as current rectifiers [2–4], logic elements [5, 6], or single photon detectors [7].

In this work we demonstrate vortex jamming effect through long-range manipulation of Abrikosov vortices in mesoscopic superconducting wires. Non-local vortex flow is initiated by applying a Lorentz force on parts of the vortex lattice, while observing vortex motion in areas where no external force is present. The nonlocal flow is due to the finite elasticity of the vortex lattice, *i.e.* finite tilt modulus  $c_{44}$  [8], compression  $c_{11}$  and shear  $c_{66}$  moduli [9–11]. Enhanced rigidity of the vortex lattice (*i.e.* enhanced  $c_{11}$  and  $c_{66}$ ) in mesoscopic superconductors with reduced dimensionality (superconducting strips) leads to the possibility of non-local manipulation of vortices on the order of several hundred vortex lattice spacings [9, 12, 13]. Non-local vortex manipulation opens opportunities to sense perturbations of the vortex system far from the point where the external force acts on an individual vortex. This dramatically increases the sensitivity to dynamic properties of Abrikosov vortices in mesoscopic superconductors.

Here we show that long-range manipulation of vortices in low- $\kappa$  materials, such as Nb, can be exploited to study granular-like properties of vortex matter, including vortex jamming [14, 15]. Reduction or complete termination of vortex flow due to strong vortex-vortex interaction in constricted (funnel) geometries leads to a reduction of dissipation due to vortex movement. Similar to granular materials, the affinity to jam in funnel geometries is most

pronounced at high particle densities, *i.e.* in our case at high magnetic fields. We examine the jamming effect in the case of a single constriction that is much larger than the size of a vortex. Vortices are channelled into a constriction on the order of few vortex cores wide [15]. We show that the vortex mobility is asymmetric with respect to the direction of motion of the vortices, as observed by the nonlocal voltage in Nb bridges, and discussed theoretically by Vodolazov et al. [12]. The experimental evidence of granular-like behavior of vortex matter that we show in this paper should initiate wider application of theoretical concepts developed in the physics of granular materials to the behavior of superconducting vortices. Based on these concepts, the engineering of pinning landscapes that suppress vortex motion via jamming will lead to lower dissipation at high magnetic fields in a wide range superconducting devices and wires.

The 100-nm-thick Nb film was sputtered using a *dc* magnetron on a silicon wafer covered with 500 nm of silicon nitride. The critical temperature of the as-grown, high quality Nb film was 9.1 K with transition width of 50mK and residual resistivity ratio  $RRR_{sim5}$ . We used e-beam lithography and reactive ion etching (combination of  $CF_4$  and  $SF_6$  plasma) to define structures similar to those shown in the inset of Figure 1. The 200-nm wide bridge had the normal state resistance of  $8.65 \mu\Omega\text{cm}$ . Considering that the slope  $dH_{c2}/dT$  near  $T_c$  is 0.4 T/K and the fact that we are in the dirty limit, we obtain the basic Ginzburg-Landau superconducting parameters of the structure: the coherence length  $\xi(0) = 13.5$  nm and the penetration depth  $\lambda(0) = 145$  nm, resulting in  $\kappa = \lambda(0)/1.63\xi(0) = 6.6$  [16].

The choice of material was motivated by the requirement of strongly interacting vortex matter in order to reduce the compressibility of the lattice and enhance the vortex jamming effects. This can be accomplished by enhancement of the elasticity moduli of the vortex lattice, which led us to use type-II superconductors with small values of  $\kappa = \lambda/\xi$  [17]. However, the intrinsic pinning in such thin films is strong due to the same reasons, and the

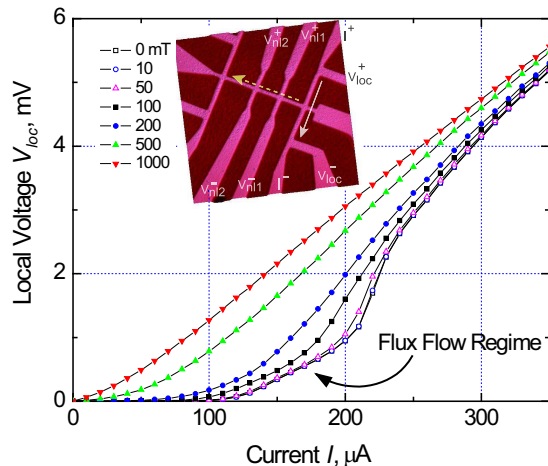


FIG. 1. (Color online) Local current-voltage characteristics of the Nb bridge at 2 K. Inset: atomic force microscopy image of the device used in the studies of nonlocal vortex movement -  $I$  - local current,  $V_{loc}$  - local voltage,  $V_{nl1}$  and  $V_{nl2}$  - nonlocal voltage leads. The distance between  $I$  and  $V_{nl1}$  and  $V_{nl2}$  at the central vortex guide channel is  $1.5 \mu\text{m}$  and  $3 \mu\text{m}$ , respectively.

vortex-pin interaction usually dominates over the vortex-vortex interaction. Therefore, the quality of the Nb thin film as well as precise definition of the mesoscopic structures are both important.

The Nb films were patterned into multi-terminal structures, as shown in the inset of Fig. 1. Direct current was applied through terminals  $I$ , and a local voltage was measured via terminals  $V_{loc}$  (conventional four-terminal geometry), while the non-local voltage was measured via terminals  $V_{nl1}$  and  $V_{nl2}$  using a Keithley 2182 nanovoltmeter. The distance between the local leads to the  $V_{nl1}$  is  $1.5 \mu\text{m}$  and to the  $V_{nl2}$  is  $3.0 \mu\text{m}$ . The center superconducting line with width  $w = 200 \text{ nm}$  serves as a guiding channel for Abrikosov vortices. When the external magnetic field is applied perpendicular to the plane of the film, vortices are nucleated in the superconducting pads located at either side of the sample, and depending on the direction of the current and the polarity of the vortices, the vortices can be moved either to the left or to the right side of the sample under the influence of Lorentz force. The coupling of the left and right superconducting Nb pads with the vortex guiding channel is through asymmetric constrictions. In case of granular-like behavior of the vortices, the funnel provides a well-defined guided concentrator for vortex movement to the right, facilitating vortex jamming [14].

The geometry of the structure is such that the applied current is confined to the current lead  $I$  and exerts a direct force on the vortices that are only in that part of the structure. The applied current decays exponentially  $\propto \exp(-\pi x/w)$  in the vortex guiding channel at a distance  $x$  away from the intersection between the lo-

cal current lead and the vortex channel [9]. Therefore, no voltage is expected at both  $V_{nl1}$  and  $V_{nl2}$  when the structure is either in the normal or in superconducting state without vortex flow.

Local current-voltage characteristics at 2 K in an applied magnetic field show that we can isolate the vortex flux-flow regime in the range of currents between  $100\text{-}200 \mu\text{A}$  (Fig. 1). The flux flow regime in this part of the vortex phase diagram is characterized by high vortex velocities [18]. The onset of the linear regime at  $\sim 100 \mu\text{A}$  can be interpreted as dynamic phase transition [19] from plastic flow at  $I \lesssim 100 \mu\text{A}$  to a coherent movement of the vortex lattice as a whole at  $I \gtrsim 100 \mu\text{A}$ .

The magnetic field dependence of the nonlocal voltage is shown in Fig. 2a. The current of  $150 \mu\text{A}$  was applied through the structure in order to initiate the flux flow through the superconducting vortex guiding channel. The nonlocal voltage appears at nonzero magnetic field, reaches some finite value and then disappears at higher magnetic fields approaching  $H_{c2}$  at this temperature. The voltage signal shown in this figure is obtained by taking a difference in voltage signals for opposite directions of the applied current thus eliminating any thermal emf. The signal is symmetric about zero magnetic field. With increasing distance from the driving current the non-local voltage is reduced, but it is still finite even  $3 \mu\text{m}$  away. The non-local voltage decays with distance from the current lead where Lorentz force is present. If the vortex lattice was ideally rigid the non-local voltage would not decay with distance. But finite rigidity of the vortex lattice causes local compression of the lattice and presence of disorder in the film causes finite pinning. Both of these contribute to loss of vortex flow along the vortex carrying stripe and decay of non-local voltage with distance.

One stark difference from earlier reports on the nonlocal vortex motion is the appearance of highly symmetric peaks and kinks in the nonlocal voltage at specific values of the magnetic field. The features are correlated between the first and second nonlocal probe, indicating highly correlated, long-range vortex flow along the channel. The main features in the nonlocal voltage curves can be observed at 190, 435, 730, and 1070 mT. Weakly pronounced features, such as kinks, are present at intermediate fields, and they correlate between the two non-local voltage signals. Considering the mesoscopic size of the vortex channel the main peaks are to be associated with transitions between structural configuration of the moving vortex lattice in the channel. The narrow width of the channel that is on the order of the vortex-vortex spacing imposes its 1D geometry on the vortex lattice. A triangular vortex lattice re-organizes into a vortex chain structure [20–22]. Since the driving current is strong, such that the vortex lattice is moving with relatively high speed, the vortex lattice can be considered dynamically ordered [19] and its configuration can be calculated

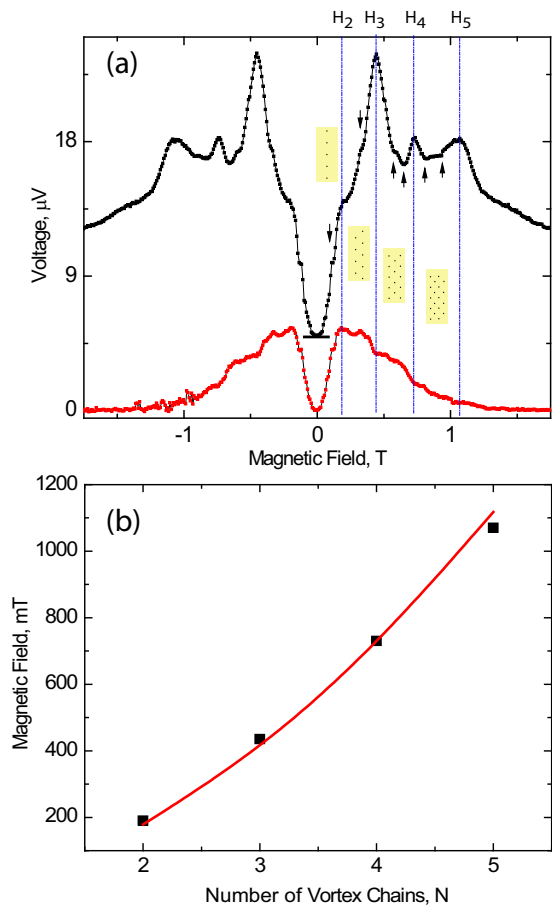


FIG. 2. (Color online) (a) Nonlocal voltage as a function of applied magnetic field measured in the 200-nm-wide channel at a distance of  $1.5 \mu\text{m}$  ( $V_{nl1}$  - black) and  $3 \mu\text{m}$  ( $V_{nl2}$  - red) from the applied current. The curves are shifted vertically for clarity. Blue vertical dotted lines correspond to magnetic fields at which vortex chain transitions take place with schematic of vortex chain configurations at different field intervals. Arrows denote additional kinks in  $V_{nl}(H)$  dependence; (b) magnetic field dependence of the vortex chain transitions in the channel showing experimental values (points) and theoretical curve from Eq. (1). No fitting parameters are used.

by applying equilibrium conditions. At fields below  $H_2$  the vortices are arranged in a regular chain moving with steady velocity along the center axis of the mesoscopic channel. A Bean-Livingston barrier aligns the vortices in the center of the channel. When the magnetic field is increased, the intervortex spacing in the chain reduces gradually, until the intervortex distance becomes on the order of the half of strip width. At field  $H_2$  a structural transformation occurs - the vortex chain is suddenly split into two chains and the intervortex distance within each chain increases. This leads to a rapid increase of the total amount of vortices flowing through the channel leading to a peak in nonlocal voltage. Further increase in magnetic field preserves the two-chain configuration while grad-

ually decreasing the intervortex spacing within each of the chains. The process of chain splitting repeats at  $H_3$  and  $H_4$  with formation of three and four vortex chains, respectively with a corresponding peak in the nonlocal voltage. Ginzburg-Landau calculations [20] show that the magnetic fields at which the equilibrium reordering of the vortex lattice occurs are:

$$\mu_0 H_N = \frac{\sqrt{3} \Phi_0 \lambda_{ab}}{2 \lambda_c} \left( \frac{N}{w} \right)^2 \quad (1)$$

where  $\lambda_{ab}$  and  $\lambda_c$  are the in-plane and out-of-plane penetration depths, respectively,  $\Phi_0$  is the magnetic flux quantum,  $w$  is the width of the strip, and  $N=2,3,4,\dots$  is the peak index. Since Nb film is in dirty superconducting limit, the anisotropy  $\lambda_{ab}/\lambda_c \gg 1$ . The correspondence of the peaks to the theoretical model is shown in Fig. 2b. The slight discrepancy at higher order peaks might be due to the renormalization of the Bean-Livingston barrier at high fields, which would result in a slight change of the effective vortex channel width  $w$ .

Additional more weakly pronounced kinks in the nonlocal voltage can be observed at magnetic fields that are between the  $H_N$  vortex transitions. In order to elucidate the nature of these additional features we go back to the origin of the nonlocal voltage. The nonlocal voltages  $V_{nl1}$  and  $V_{nl2}$  shown in Figure 2a are the average absolute voltages induced by positive and negative driving currents  $I^+$  and  $I^-$  in the current channel, i.e.  $V_{nl}(H) = \frac{V_{nl}(I^+, H) - V_{nl}(I^-, H)}{2}$ . The  $V_{nl1}$  and  $V_{nl2}$  signals are dominated by the vortex flux flow in the central channel and any asymmetries of vortex motion up and down the channel are averaged out. In Fig. 3 we show the traces of the original  $V_{nl2}(I^+, H)$  and  $V_{nl2}(I^-, H)$  from Fig. 2a. There are two distinct features in these curves. First, the signal is symmetric with respect to simultaneous inversion of field and driving current, showing that there is an easy vortex flow direction that is independent on vortex polarity (vortices and antivortices flow easier in the same direction). Second, additional periodic kinks become more pronounced in the easy vortex flow direction.

The reason for the voltage asymmetry is due to the asymmetric geometry of the structure - the vortex guiding channel is coupled to the left and right endpoints through a different geometry. The superconducting pads that couple to the vortex guiding channel serve as vortex reservoirs that source vortices to the channel or drain the vortices from the channel. On the left end we have the funnel-shaped constriction and on the right end there is a square superconducting pad. The ability for the vortices to enter into the channel from these two pads is different; the funnel is designed to jam the vortices as they enter the 1D channel. The situation corresponds to the closed end channel described in [12]. Jamming that occurs for vortices entering the channel at the funnel end, causes reduction in vortex chain mobility in the channel and the

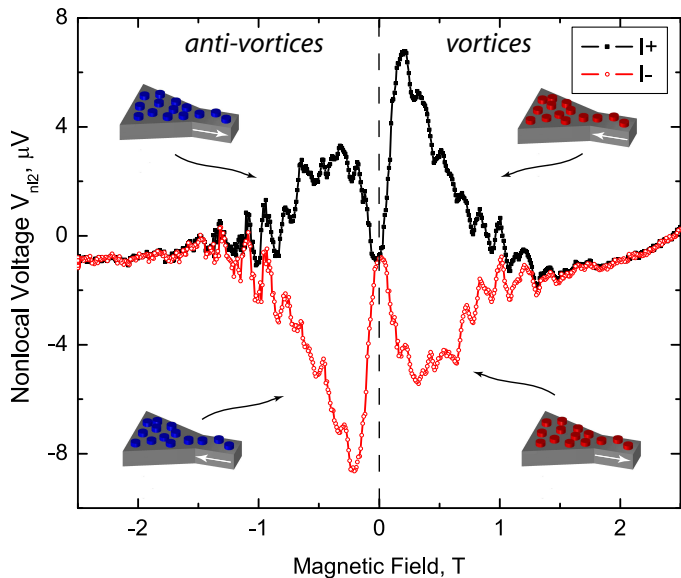


FIG. 3. (Color online) Non-local voltage  $V_{nl2}(I, H)$  as a function of the applied magnetic field for two opposite directions of the driving current ( $T=2.4$  K). Vortices of opposite polarities exhibit the same rectification behavior when moving in the same direction.

asymmetry of the  $V_{nl}$  with respect to the driving current. The same reduction will take place for vortices of opposite polarity (antivortices) subject to opposite driving current, as observed in Fig. 3. The results are similar if one drives the vortices through the channel by applying the Lorentz force with a supercurrent through the left-most pair of contacts shown in the inset of Fig. 3.

Furthermore, the mobility of the vortex chains in the channel will be dependent on the matching of the vortex structure in the source/drain pads and the channel. Matching of the vortex configurations in the channel (vortex chains) to the vortex configuration in the pads (vortex lattice) would cause higher vortex mobility (larger  $V_{nl}$ ) due to easier entrance/exit of vortices, while non-matching configurations will cause reduction in  $V_{nl}$ . In our experiments, when we are using the right pad (square) as a source of vortices going into the channel, we observe higher  $V_{nl}$ . We also observe more pronounced periodic peaks in  $V_{nl}$  corresponding to the geometrical matching effect between the square vortex lattice in the pad and the vortex chain structure in the channel. Further theoretical work could, possibly correlate with these matching configurations.

In conclusion, we have studied the dynamics of non-local Abrikosov vortex flow in mesoscopic superconducting Nb channels. High rigidity of the vortex lattice in this material is responsible for quasi-1D long-range correlated vortex movement. The magnetic field dependence of the non-local voltage induced by the flux flow shows that vortices form ordered vortex chains. Voltage asymmetry (rectifying effect) with respect to the direction of

vortex flow is evidence that vortex jamming can significantly moderate vortex dynamics in mesoscopic geometries. The finding can be applied to future devices exploiting vortex dynamics and vortex manipulation [23].

We would like to thank Ralu Divan (CNM, Argonne) for assistance in preparation of the samples. This work as well as the use of the Center for Nanoscale Materials and the Electron Microscopy Center at Argonne National Laboratory were supported by UChicago Argonne, LLC, Operator of Argonne National Laboratory (“Argonne”). Argonne, a U.S. Department of Energy Office of Science laboratory, is operated under Contract No. DE-AC02-06CH11357. M.I. would like to acknowledge the support of U.S. Department of Energy under Grant No. de-sc0004556.

\* e-mail: goran@drexel.edu

† Present address: San Jose Research Center, Hitachi Global Storage Technologies, San Jose, CA 95135

- [1] A. M. Campbell and J. E. Evetts, *Adv. Phys.* **21**, 199 (1972).
- [2] J. Van de Vondel, C. C. de Souza Silva, B. Y. Zhu, M. Morelle, and V. V. Moshchalkov, *Phys. Rev. Lett.* **94**, 057003 (2005).
- [3] K. Yu, T. W. Heitmann, C. Song, M. P. DeFeo, B. L. T. Plourde, M. B. S. Hesselberth, and P. H. Kes, *Phys. Rev. B* **76**, 220507 (2007).
- [4] K. Yu, M. B. S. Hesselberth, P. H. Kes, and B. L. T. Plourde, *Phys. Rev. B* **81**, 184503 (2010).
- [5] M. B. Hastings, C. J. O. Reichhardt, and C. Reichhardt, *Phys. Rev. Lett.* **90**, 247004 (2003).
- [6] T. Puig, E. Rosseel, M. Baert, M. J. V. Bael, V. V. Moshchalkov, and Y. Bruynseraede, *Appl. Phys. Lett.* **70**, 3155 (1997).
- [7] A. M. Kadin, M. Leung, and A. D. Smith, *Phys. Rev. Lett.* **65**, 3193 (1990).
- [8] I. Giaever, *Phys. Rev. Lett.* **15**, 825 (1965).
- [9] I. V. Grigorieva, A. K. Geim, S. V. Dubonos, K. S. Novoselov, D. Y. Vodolazov, F. M. Peeters, P. H. Kes, and M. Hesselberth, *Phys. Rev. Lett.* **92**, 237001 (2004).
- [10] N. Kokubo, R. Besseling, V. M. Vinokur, and P. H. Kes, *Phys. Rev. Lett.* **88**, 247004 (2002).
- [11] N. Kokubo, T. G. Sorop, R. Besseling, and P. H. Kes, *Phys. Rev. B* **73**, 224514 (2006).
- [12] D. Y. Vodolazov, F. M. Peeters, I. V. Grigorieva, and A. K. Geim, *Phys. Rev. B* **72**, 024537 (2005).
- [13] A. Helzel, I. Kokanović, D. Babić, L. V. Litvin, F. Rohlfing, F. Otto, C. Sürgers, and C. Strunk, *Phys. Rev. B* **74**, 220510 (2006).
- [14] C. J. O. Reichhardt and C. Reichhardt, *Phys. Rev. B* **81**, 224516 (2010).
- [15] C. Reichhardt and C. O. Reichhardt, *Physica C* **470**, 722 (2010), ISSN 0921-4534.
- [16] P. H. Kes and C. C. Tsuei, *Phys. Rev. B* **28**, 5126 (1983).
- [17] A. M. Campbell, *J. Phys. C* **2**, 1492 (1969).  
A. M. Campbell, *J. Phys. C* **4**, 3186 (1971).  
E. H. Brandt, *Rep. Prog. Phys.* **58**, 1465 (1995).  
G. Blatter, M. V. Feigel'man, V. B. Geshkenbein, A. I.

- Larkin, and V. M. Vinokur, *Rev. Mod. Phys.* **66**, 1125 (1994).
- [18] C. Peroz and C. Villard, *Phys. Rev. B* **72**, 014515 (2005).
- [19] A. E. Koshelev and V. M. Vinokur, *Phys. Rev. Lett.* **73**, 3580 (1994).
- [20] S. Brongersma, E. Verweij, N. J. Koeman, D. G. de Groot, R. Griessen, and B. I. Ivlev, *Thin Solid Films* **228**, 201 (1993).  
S. Brongersma, E. Verweij, N. J. Koeman, D. G. de Groot, R. Griessen, and B. I. Ivlev, *Phys. Rev. Lett.* **71**, 2319 (1993).
- [21] J. Guimpel, L. Civale, F. de la Cruz, J. M. Murduck, and I. K. Schuller, *Phys. Rev. B* **38**, 2342 (1988).
- [22] S. Takács, *Czech. J. Phys. B* **28**, 1260 (1978).  
C. Carter, *Canad. J. Phys.* **47**, 1447 (1969).  
G. Carneiro, *Phys. Rev. B* **57**, 6077 (1998).  
D. Luzhbin, *Phys. Solid Stat.* **43**, 1823 (2001).  
E. Bronson, M. P. Gelfand, and S. B. Field, *Phys. Rev. B* **73**, 144501 (2006).
- G. Karapetrov, J. Fedor, M. Iavarone, D. Rosenmann, and W. K. Kwok, *Phys. Rev. Lett.* **95**, 167002 (2005).  
G. Karapetrov, M. V. Milošević, M. Iavarone, J. Fedor, A. Belkin, V. Novosad, and F. M. Peeters, *Phys. Rev. B* **80**, 180506 (2009).
- [23] H. Bartolf, A. Engel, A. Schilling, K. Il'in, M. Siegel, H.-W. Hübbers, and A. Semenov, *Phys. Rev. B* **81**, 024502 (2010).